# Statistical modeling of in situ hiss amplitudes using ground measurements

D. I. Golden,[1] M. Spasojevic,[1] W. Li,[2] and Y. Nishimura[2]

Received 14 November 2011; revised 26 March 2012; accepted 27 March 2012; published 10 May 2012.

[1] Plasmaspheric hiss is a naturally occurring extremely low frequency electromagnetic emission that is often observed within the Earth's plasmasphere. Plasmaspheric hiss plays a major role in the scattering and loss of electrons from the Earth's radiation belts, thereby contributing to the maintenance of the slot region between the inner and outer electron belt. Traditionally, in situ satellite observations have been the measurement modality of choice for studies of plasmaspheric hiss due to their ability to directly measure the hiss source region. However, satellite studies are relatively short-lived and very few satellite receivers remain operational for an entire 11-year solar cycle. Ground stations, in contrast, may collect multiple solar cycles' worth of data during their lifetime, yet they cannot directly measure the hiss source region. This study aims to determine the extent to which measurements of hiss at midlatitude ground stations may be used to predict the mean amplitude of in situ measurements of plasmaspheric hiss. We use coincident measurements between Palmer Station, Antarctica ($L$ = 2.4, 50°S invariant latitude) and the THEMIS spacecraft from June 2008 through May 2010, during solar minimum. Using an autoregressive multiple regression model, we show that in the local time sector from 00 < MLT < 12, when the ionosphere above Palmer Station is in darkness and hiss is observed at Palmer, the amplitude of plasmaspheric hiss observed by the THEMIS spacecraft is 1.4 times higher than when hiss is not observed at Palmer. In the same local time sector when the ground station is in daylight and hiss is observed, the THEMIS observed amplitudes are not significantly different from those when hiss is not observed on the ground. A stronger relationship is found in the local time sector from 12 < MLT < 24 where, when Palmer is in daylight and hiss is observed, THEMIS plasmaspheric hiss amplitudes are 2 times higher compared to when hiss is not observed at Palmer. There are insufficient statistics for the 12 < MLT < 24 sector during nighttime conditions. These results suggest that hiss emissions observed at Palmer in the dusk sector are likely plasmaspheric hiss, while those observed in the dawn sector may in fact be an emission other than plasmaspheric hiss, such as either ELF hiss or dawn chorus which has originated at high $L$-shells. Though these results suggest that ground measurements of plasmaspheric hiss are not likely to be a viable replacement for in situ measurements, we believe that the predictive ability of our 12 < MLT < 24 sector model may be improved by including measurements taken during geomagnetically disturbed intervals that are characteristic of solar maximum.

**Citation:** Golden, D. I., M. Spasojevic, W. Li, and Y. Nishimura (2012), Statistical modeling of in situ hiss amplitudes using ground measurements, *J. Geophys. Res.*, *117*, A05218, doi:10.1029/2011JA017376.

## 1. Introduction

[2] Plasmaspheric hiss is a naturally occurring extremely low frequency (ELF) electromagnetic emission that is often observed within the plasmasphere in the near-Earth magnetosphere. The source mechanism of hiss is an area of active research, but the three most likely candidates include the cyclotron resonant amplification of natural wave turbulence [*Kennel and Petscheck*, 1966; *Kennel and Thorne*, 1967; *Thorne et al.*, 1973, 1979; *Church and Thorne*, 1983], whistlers generated by terrestrial lightning [*Sonwalkar and Inan*, 1989; *Draganov et al.*, 1992; *Green et al.*, 2005; *Meredith*

[1]Electrical Engineering Department, Stanford University, Stanford, California, USA.
[2]Department of Atmospheric and Oceanic Sciences, University of California, Los Angeles, California, USA.

Corresponding author: D. I. Golden, Electrical Engineering Department, Stanford University, 350 Serra Mall, Packard Bldg., Stanford, CA 94305-9515, USA. (dgolden1@stanford.edu)


0148-0227/12/2011JA017376

*et al.*, 2006a] or magnetospheric ELF/VLF chorus [*Parrot et al.*, 2004; *Santolík et al.*, 2006; *Bortnik et al.*, 2008, 2009]. Hiss has been implicated as a major driving force for the loss of energetic electrons in the Earth's radiation belts [e.g., *Lyons et al.*, 1972; *Lyons and Thorne*, 1973; *Abel and Thorne*, 1998; *Meredith et al.*, 2006b, 2007, 2009]. As such, radiation belt models require accurate estimates of hiss amplitude in order to plausibly model the dynamics of the radiation belts.

[3] In situ measurements of hiss have long been the gold standard for measuring the distribution of hiss in the plasmasphere, from early statistical studies using the OGO satellites [e.g., *Dunckel and Helliwell*, 1969; *Russell et al.*, 1969; *Thorne et al.*, 1973], to more recent studies using the CRRES satellite [e.g., *Meredith et al.*, 2004]. Despite the relative popularity of in situ studies, hiss was originally discovered using ground measurements [e.g., *Storey*, 1953], and many long-term ground measurements of hiss are ongoing today [e.g., *Smith et al.*, 2010; *Golden et al.*, 2011]. There is a long-held belief that plasmaspheric hiss, unlike some other whistler mode magnetospheric waves such as chorus and whistlers, cannot be observed on the ground [*Sonwalkar*, 1995, section 4.2.1.1] due to theoretical considerations of magnetospheric reflection near the local lower hybrid resonance frequency [*Thorne and Kennel*, 1967] and the low-frequency cutoff between the proton and helium gyrofrequencies [*Gurnett and Burns*, 1968]. However, it was shown by *Golden et al.* [2009] that hiss emissions are often seen at Palmer Station, Antarctica ($L = 2.4$), suggesting that plasmaspheric hiss may in fact regularly propagate to the ground.

[4] One major advantage that ground stations have over satellites in the measurement of hiss is the longevity of ground stations. The British Antarctic Survey operated the ELF/VLF VELOX receiver at Halley Station, Antarctica ($L = 4.5$) for nearly 16 continuous years from 1992 to 2007 [*Smith et al.*, 2010]. Data from Halley was used to infer the presence of hiss from the local time and frequency distribution of wave power in the VELOX receiver's eight wideband channels. Stanford University operates a broadband ELF/VLF receiver at Palmer Station, which has been recording digital data since 2000; analog recordings at Palmer extend back another decade. *Golden et al.* [2011] analyzed the digital full-resolution broadband Palmer data using an automated emission detector to produce a 10-year database of spectrally categorized chorus and hiss emissions from May 2000 through May 2010. It is relatively rare, in contrast, for satellite receivers to remain operational for a solar cycle.

[5] At Palmer, the most prevalent hiss emissions appear in the dawn and dusk sectors below 1 kHz in frequency, with a frequency and local time dependence consistent with plasmaspheric hiss. Hiss emissions with frequencies 1–4 kHz are also observed in the dusk sector, but they are less common than the lower frequency hiss; the frequencies of these hiss emissions are more consistent with midlatitude hiss (see *Golden et al.* [2009, section 1] for a review of different types of magnetospheric hiss). Throughout this study, we do not explicitly distinguish between different types of hiss at Palmer; we define hiss at Palmer as any observed emissions which is incoherent and exhibits no obvious structure in its frequency-time behavior.

[6] Though the long operational duration of ground stations can result in a great trove of data for use in statistical studies, the fact that they are engaged in remote, rather than in situ sensing can complicate the interpretation of the data. Due to cross-$L$ and sub-ionospheric propagation of waves, ground stations are capable of observing waves which may originate from $L$-shells distant from those of the station [e.g., *Golden et al.* 2010]. Additionally, ground stations are intrinsically limited to sampling the portion of magnetospheric waves that are able to propagate to low altitudes and penetrate through the ionosphere [e.g., *Sonwalkar*, 1995, pp. 424–425]. These measurable waves include waves that have undergone minimal damping en route from their magnetospheric source region, and that have propagated such that their wavenormals are either within the transmission cone at the ionospheric boundary [*Helliwell*, 1965, section 3.7] or that have scattered into the transmission cone from low-altitude ionospheric density irregularities. Thus, not all waves which exist in space are observable on the ground, and ground measurements of waves are limited to serving as proxy measurements of the magnetospheric environment.

[7] Variable ionospheric and magnetospheric conditions make it difficult to interpret the observed waves on the ground in the context of their magnetospheric source based on physical models. It is of great interest, therefore, to determine statistically the extent to which waves observed on the ground may reflect the actual wave environment in the magnetosphere. If ground measurements are found to be an effective proxy for in situ measurements, this would allow ground measurements to be incorporated into many studies for which only in situ measurements are currently deemed acceptable. This would decrease our reliance on expensive and relatively uncommon satellite missions for magnetospheric wave research, and allow ground networks to be used to greatly increase our ability to collect statistics of magnetospheric waves. Knowledge of these waves, and of plasmaspheric hiss in particular, are essential for the understanding of radiation belt dynamics.

[8] This study seeks to statistically determine the relationship between hiss emissions observed on the ground at Palmer Station, Antarctica, and those observed on the Time History of Events and Macroscale Interactions during Substorms (THEMIS) constellation of satellites.

## 2. Instrumentation and Data

[9] For this study, data was used from the inner magnetospheric THEMIS satellites (probes A, D and E) and Palmer Station from June 2008 through May 2010, near solar minimum at the beginning of solar cycle 24. Because the measurements were conducted during solar minimum, geomagnetic activity, and therefore hiss occurrence and observed amplitude, was also minimized. Thus, our results should be interpreted as being strictly valid only during solar minimum. We speculate on how results may differ for data collected during solar maximum in section 5.

### 2.1. THEMIS

[10] The THEMIS mission is composed of five separate probes in near-equatorial orbits with apogees above 10 $R_E$ and perigees below 2 $R_E$ [*Angelopoulos*, 2008]. The Digital

Fields Board (DFB) [*Cully et al.*, 2008] calculates the mean amplitude of the electric and magnetic field in 6 logarithmically spaced frequency bands from 0.1 Hz to 4 kHz using electric field data from the double-probe Electric Fields Instrument (EFI) [*Bonnell et al.*, 2008] and magnetic field data from the Search Coil Magnetometer (SCM) [*Roux et al.*, 2008; *Le Contel et al.*, 2008]. The resulting filter bank wave amplitude is included in the survey-mode telemetry, covering most orbits with a measurement cadence of four seconds [*Cully et al.*, 2008]. The measures of THEMIS hiss amplitude used in this study are derived exclusively from SCM survey-mode wave data.

[11] Plasmaspheric hiss is, by definition, primarily confined to the plasmasphere. It is therefore necessary to distinguish between intra and exo-plasmaspheric measurements on the THEMIS probes so as not to confuse measurements of exo-plasmaspheric emissions, such as ELF/VLF chorus, with measurements of plasmaspheric hiss. We use the approach described in section 2 of *Li et al.* [2010] to infer the local electron density from the spacecraft potential and electron thermal speed measured by the THEMIS Electric Field Instrument (EFI) and Electrostatic Analyzer (ESA) [*McFadden et al.*, 2008] instruments, respectively. Details of the method are described by *Mozer* [1973] and *Pedersen et al.* [1998]. The uncertainties associated with the derived electron densities are generally within a factor of ~2.

[12] Given the electron densities, we then follow work of past authors [e.g., *Moldwin et al.*, 1994; *Sheeley et al.*, 2001] and define

$$n_b = 10 \times \left(\frac{6.6}{L}\right)^4. \quad (1)$$

We consider regions where the total electron density is greater than or equal to the larger of $n_b$ and 50 $cm^{-3}$ to be within the plasmasphere, and all other regions to be outside the plasmasphere. Only THEMIS data recorded within the plasmasphere, as determined via this method, is used in this study.

[13] To determine observed hiss amplitude, we use the highest three recorded filter bank (FBK) levels of the first SCM channel (SCM1), which have frequency ranges of 80–227 Hz, 316–904 Hz and 1390–4000 Hz (passbank levels 4, 2 and 0, respectively, from *Cully et al.* [2008, Table 6]). Although plasmaspheric hiss is typically seen below ~2 kHz, and the highest FBK level includes measurements up to ~4 kHz, we still include this highest FBK level since we expect no other emissions to occupy this frequency bin within the plasmasphere, with the possible exception of equatorial magnetosonic waves (discussed subsequently).

[14] We have empirically determined the noise floors of SCM FBK levels 4 (80–227 Hz), 2 (316–904 Hz) and 0 (1390–4000 Hz) to be slightly below 0.96, 1.1 and 4.4 pT, respectively. We take the total hiss power to be the sum of the power of these three FBK levels, where any channel power is set to zero in the sum if it is below the empirical noise floor. If all three channels are at or below their noise floors, then the data is discarded. Additionally, at low altitudes near perigee, the SCM instrument becomes saturated due to the Earth's large static magnetic field, resulting in invalid FBK values which may be either abnormally high (>1 nT) or low (below the noise floor). We mitigate these anomalies by excluding any data collected within one minute of when either the sum of the three FBK levels is greater than 1 nT or any channel amplitude is below half of its noise floor. Note that because we use data from only one component of the magnetic field, and this component is perpendicular to the ambient magnetic field, the measured hiss amplitude is somewhat below the true amplitude by, on average, a factor of $\sqrt{2}$.

[15] Besides plasmaspheric hiss, the other emission of note which may appear with significant amplitude on the SCM data between 80–4000 Hz is equatorial magnetosonic waves. Magnetosonic waves are typically confined to within a few degrees of the equator [e.g., *Russell et al.*, 1970; *Gurnett*, 1976; *Němec et al.*, 2005] and may appear at frequencies up to the lower hybrid resonance, generally within the same frequency range as hiss inside the plasmasphere. Above the ion cyclotron frequency and below the lower hybrid frequency, magnetosonic waves are the limit of the whistler (R-X) mode of propagation for wavenormals perpendicular to the ambient magnetic field [e.g., *Lysak and Song*, 2004; *Inan and Gołkowski*, 2010, section 11.3.3]. Given either the wavenormals or the polarizations of observed waves, it would be possible to distinguish between the field-aligned or oblique, right-hand circularly polarized whistler mode waves and the perpendicularly propagating, magnetically linearly polarized magnetosonic waves. However, this is not possible in the THEMIS survey mode data, which includes only one channel each of electric and magnetic fields sampled at a cadence of four seconds. Therefore, to mitigate excessive contamination from magnetosonic waves, we exclude THEMIS measurements within four degrees of the dipole equator.

### 2.2. Palmer Station

[16] Palmer Station is located on Anvers Island, near the northernmost end of the Antarctic peninsula, at 64.77°S, 64.05°W, with IGRF geomagnetic parameters of $L$ = 2.4, $\Lambda$ = 50°S invariant latitude, and magnetic local time (MLT) = UTC − 4.0 hr at 100 km altitude. The Palmer receiver records broadband ELF/VLF data at 100 kilosamples/s using two cross-loop magnetic field antennas with 96 dB of dynamic range. The Palmer emission database used in this study consists of 10-s broadband measurements, with an inter-measurement period of 15-min at 5, 20, 35 and 50 min past the UTC hour, 24 hr per day. The start time of a measurement is referred to as a "synoptic epoch." These measurements use Palmer's North/South channel exclusively, as it suffers significantly less contamination from local noise than does the East/West channel; this is a result of the fact that the main station lies to the East of the antenna.

[17] Hiss emissions are detected automatically in the Palmer data using the automated emission detector of *Golden et al.* [2011]. The automated emission detector is designed to detect both chorus and hiss emissions and consists of three broad steps: (1) cleaning the source broadband data of common sources of interference, particularly sferics and hum, (2) detecting "events" which, before categorization, may be either emissions or noise, and (3) categorizing the detected events as noise, chorus, and hiss. The event detection step consists of a variety of heuristic methods to isolate "emission-like" spectral features from noise, and the

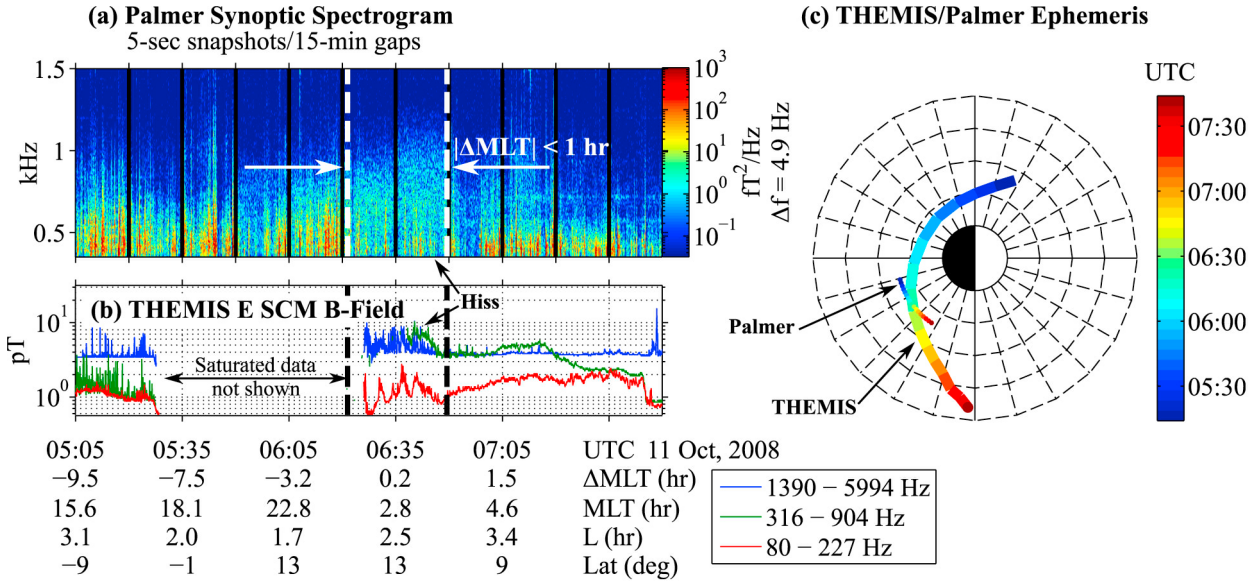


**Figure 1.** An example hiss conjunction measurement between THEMIS E and Palmer on 11 October 2008. (a) Palmer synoptic spectrogram, consisting of 5-s snapshots with 15-min gaps between each snapshot. Vertical dashed lines indicate the boundary of the conjunction, where the MLT difference between Palmer and THEMIS is less than 1 hr. (b) THEMIS E DFB SCM data for the upper three DFB frequency channels. Channel amplitudes which are saturated due to the Earth's magnetic field during perigee are not shown. (c) THEMIS E ephemeris and Palmer IGRF coordinates for this period, colored by universal time, showing the L and MLT range of the conjunction.

event categorization step uses a sequential pair of artificial neural networks to first distinguish emissions from noise and then to distinguish chorus from hiss among the emissions. Emissions are distinguished primarily based on their observed spectral features; i.e., chorus is a "bursty" emission, consisting of discrete elements, while hiss is a structureless noise-like emission. Currently, ten years of emission observations from May 2000 through May 2010 are available in the Palmer emission database, and recordings at Palmer are ongoing.

[18] Although hiss amplitude may easily be determined from the broadband data recorded at Palmer, in this study, we neglect the actual measured hiss amplitude in favor of a Boolean true/false measure of whether hiss is detected or not. We decided to use this Boolean measure instead of the real-valued hiss amplitude after observing that the correlation between the Palmer hiss amplitude and the THEMIS hiss amplitude was negligible (with correlation $p$-value of $\sim$0.65). This is a consequence of the wide variety of ways that hiss may be attenuated en route from its magnetospheric source to the ground. Hiss may experience Landau damping in the magnetosphere due to interactions with super-thermal electrons, it may experience focusing effects due to converging magnetic field lines or defocusing effects due to partial magnetospheric or ionospheric reflections, and it may suffer absorption in the ionosphere, either during its transmission through the ionosphere or while propagating in the Earth-ionosphere waveguide. As most of these factors are significant, unknown, and highly variable based on geomagnetic conditions and the hiss source region, we do not expect the amplitude between in situ hiss and ground-observed hiss to be well correlated. Our Boolean measure of "hiss/no hiss" at Palmer is a simplification that we later show to be a useful predictor of in situ hiss amplitude.

## 3. Case Study: Conjunction Hiss Measurement Between THEMIS E and Palmer on 11 October 2008

[19] To get a feel for the underlying statistics of this study, we show an example conjunction measurement of plasmaspheric hiss between the THEMIS E probe and Palmer Station in Figure 1. The simultaneous observation of plasmaspheric hiss occurred on 11 October 2008, between approximately 06:20–06:50 UTC, which is the range over which THEMIS E and Palmer were within 1 hr of each other in dipole MLT.

[20] Figure 1a shows a synoptic spectrogram of broadband data from the ELF/VLF receiver at Palmer Station. The synoptic spectrogram consists of a series of 5-s snapshots separated by 15-min gaps, stitched together to appear as a continuous spectrogram. Sferics and hum have been removed from the plotted data using the sferic removal procedure from *Golden et al.* [2011, section 2.1] and the hum removal procedure from *Cohen et al.* [2010]. The hiss emission at Palmer appears below 1 kHz and lasts from approximately 05:50–06:50 UTC. Also visible below $\sim$0.7 kHz is a steady background of sferic slowtails, which persist throughout the plotted time range.

[21] Figure 1b shows the measured THEMIS E survey-mode SCM data for the upper three FBK levels during the same interval. The THEMIS data is continuous (it does not have 15-min gaps, as the Palmer data does), with a sampling period of 4 sec. Between 05:27 and 06:26 UTC, invalid data values that were recorded when the SCM instrument was

saturated due to the Earth's DC magnetic field during perigee have been omitted. The hiss emission is seen on all three FBK levels during the period of the conjunction, defined as when THEMIS and Palmer are within 1 hr in MLT, which is marked with vertical dashed lines.

[22] Figure 1c shows the simultaneous ephemeris of THEMIS E and the IGRF $L$ and MLT of Palmer for this measurement period. The conjunction occurs in the post-midnight sector. During the plotted time period, THEMIS E sweeps out a much larger range of $L$ and MLT than does Palmer. It is important to note that, as a result of cross-$L$ and MLT propagation of emissions within the magnetosphere and subionospheric propagation of emissions within the Earth-ionosphere waveguide, ground stations are capable of observing emissions that may originate at points rather disparate from their IGRF field lines. Thus the observed hiss at Palmer need not have originated exactly on the plotted line of Palmer's IGRF $L$ and MLT, and this path is merely shown for reference.

[23] This case study, showing an instance in which hiss is observed in situ on THEMIS and propagates to the ground to be received at Palmer, is representative of the underlying statistics of simultaneous hiss observations on THEMIS and at Palmer, discussed in subsequent sections.

## 4. Statistical Modeling of Hiss Amplitude

[24] Our goal in this section is to determine the extent to which observations of hiss at Palmer may be used to predict the amplitude of hiss observed on THEMIS. We do not seek an *optimal* model of hiss amplitude on THEMIS; we are simply investigating whether ground observations could be an important component of such a model. After explaining our rationale for separating the models into those during daytime and nighttime at Palmer in section 4.1 and discussing our statistical database of THEMIS data in section 4.2, we show how THEMIS hiss amplitude may predict the occurrence of hiss at Palmer in section 4.3; this is modeling in the forward direction, beginning with the waves' origins in space and concluding with their reception on the ground. This is followed by the core component of this study, a model to determine whether Palmer hiss observations are useful in estimating THEMIS hiss amplitude in section 4.4; this "reverse" modeling has practical applications for using cheap and robust ground measurements to estimate hiss properties in space.

### 4.1. Separating Observations at Palmer by Daytime/Nighttime and MLT

[25] Due to diurnal variations in the propagation characteristics of ground-observed waves, it is necessary to separately consider Palmer observations for local day and local night. As is true of all ELF/VLF ground receivers, measured wave amplitude at Palmer is strongly influenced by absorption in the ionosphere. At times when the ionosphere in Palmer's vicinity is in darkness, the plasma density in the ionosphere is at a minimum, which results in a minimum of both trans-ionospheric absorption and of sub-ionospheric propagation loss [e.g., *Smith and Jenkins*, 1998]. We would therefore expect that magnetospheric waves observed during local day at Palmer are less common and of lower mean amplitude than those observed during local night.

[26] An intuitive way to visualize local time dependence of hiss observed at Palmer, and, by extension, the effect of the day/night terminator, is via the "cumulative spectrogram" plot [*Golden et al.*, 2009, section 2.2]. The cumulative spectrogram is the logarithmic sum of the average power spectral density (PSD) of each hiss measurement, divided by the number of available measurements for each synoptic epoch. This is effectively a plot of normalized emission occurrence, weighted by emission PSD, with respect to frequency and local time. In the case of the Palmer ground data, the PSD is estimated via a modified version of the Welch periodogram which we call the "mediogram" [*Golden et al.*, 2011, section 2.2]. The mediogram can be thought of as the median of the columns of a spectrogram (i.e., the median PSD over time), as opposed to the Welch periodogram which is the mean of the spectrogram columns. The mediogram is used in lieu of the Welch periodogram to minimize contribution to the PSD estimate from impulsive sferics from terrestrial lightning.

[27] The discrepancy between received hiss amplitude during local day and night can be most easily seen when examining cumulative spectrograms of the Palmer hiss database broken down by month. Figure 2 shows cumulative spectrograms of hiss observed at Palmer for each month, averaged over the 10 years of data available in the Palmer emission database from May 2000 through May 2010. In each cumulative spectrogram, frequency increases radially from 400 Hz on the outside to 3 kHz on the inside of the circle. Midnight is to the left, and MLT increases azimuthally in the counterclockwise direction. The dawn terminator at 100 km altitude during the middle of each month is indicated with golden radial bars in each spectrogram and the dusk terminator is indicated with blue radial bars. Times when Palmer is in local daylight are indicated with golden highlights around the outer circumference of each spectrogram, and times when Palmer is in local darkness are indicated with blue highlights. In this figure, as in the remainder of this paper, Palmer is considered to be in daylight if the point at Palmer's geographic location at 100 km altitude is sunlit, and it is considered to be in darkness otherwise.

[28] Because Palmer is in the southern hemisphere, it experiences the Austral seasons. Austral summer (December, January, February) has characteristically long days, and the ionosphere is sunlit for 24 hrs per day in these months. In Austral winter (June, July, August), the station experiences a minimum number of hours of daylight, though the ionosphere is still sunlit for nearly 12 hours of each day. It can be seen in Figure 2 that hiss is preferentially observed during darkness at all MLTs, with the exception of midnight and noon. Hiss is infrequently observed at midnight because it is less prevalent in the magnetosphere at midnight (as will be discussed in section 4.2), and hiss is infrequently observed near noon due to those hours being sunlit all year at Palmer. The discrepancy between darkness and daylight observations of hiss is simply a result of increased ionospheric absorption during local day. In this study, we separately consider models where the ionosphere at 100 km altitude above Palmer is (1) in darkness or (2) in daylight.

[29] Due to fact that observed hiss amplitude and occurrence are at a minimum at Palmer at noon and midnight, the observed hiss at Palmer exhibits a bimodal distribution in MLT. This is illustrated in Figure 3, which shows cumulative

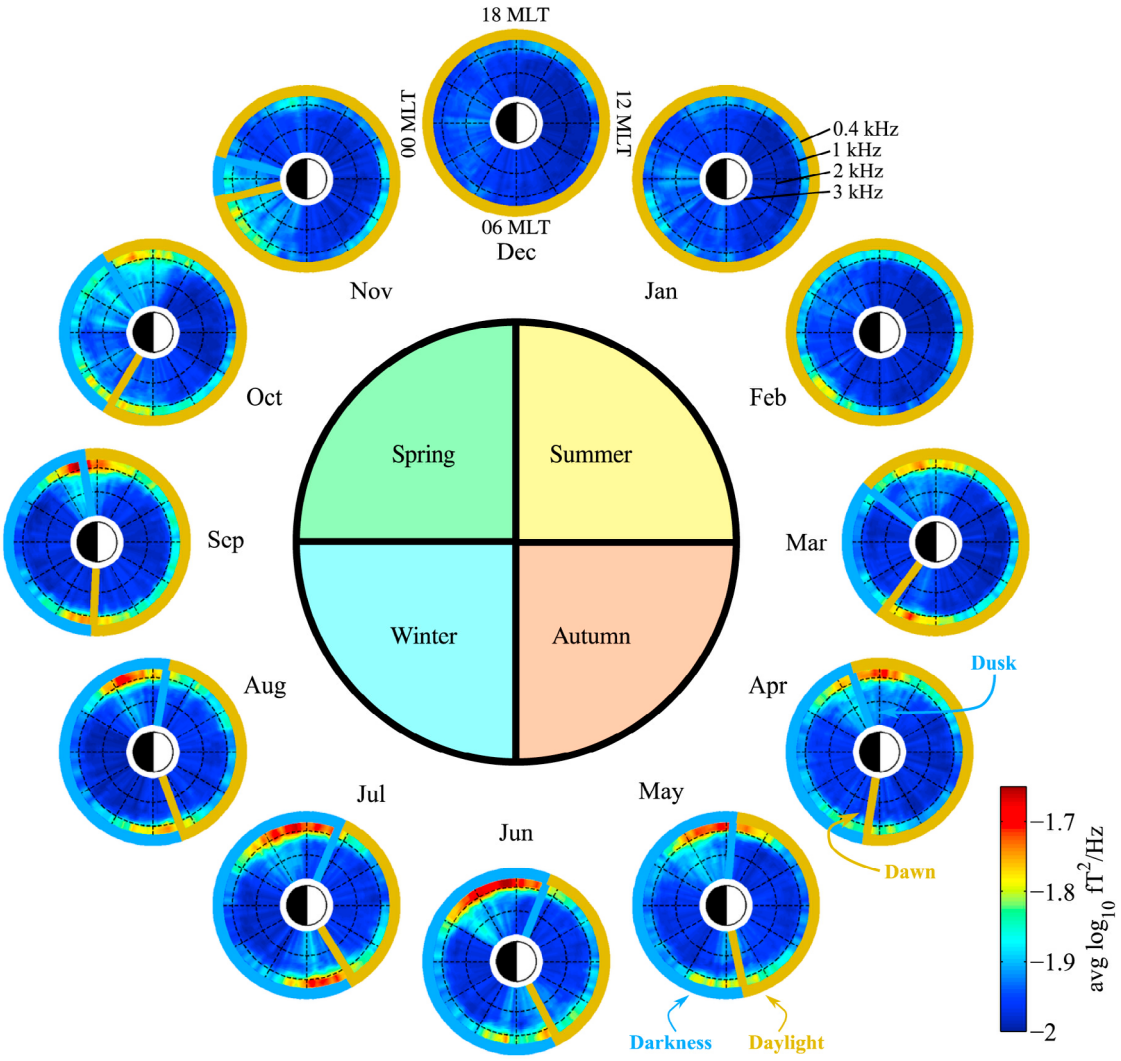


**Figure 2.** Radial cumulative spectrograms showing the MLT and frequency dependence of plasmaspheric hiss as observed at Palmer during different months of the year from 2000–2010. Frequency increases with decreasing radius, from 0.4 kHz to 3 kHz, and MLT increases from midnight counterclockwise from the left. Times when the ionosphere at 100 km altitude above Palmer is in daylight or darkness are indicated with golden and blue highlights around the circumference of each spectrogram, averaged for each month. Hiss is seen less often and with lower amplitude during local daylight due to increased trans-ionospheric and sub-ionospheric attenuation of waves when the ionospheric is sunlit.

spectrograms, averaged over all months and years from May 2000 through May 2010, of both chorus and hiss at Palmer (this figure is analogous to Figure 7 of *Golden et al.* [2011]). As in Figure 2, these chorus and hiss emissions were detected using the automated technique of *Golden et al.* [2011]. Peaks in the hiss distribution are seen at dawn at 05 MLT and at dusk at 19 MLT, separated by minimums at noon and midnight. Chorus peaks in the dawn sector, around 07 MLT. Because of the overlap in chorus and hiss distributions in the range 00 < MLT < 12, we also separately consider models for the MLT ranges (1) 00 < MLT < 12 and (2) 12 < MLT < 24.

### 4.2. THEMIS Average Hiss Amplitude and Statistics

[30] In order to gain insight into how hiss amplitude varies with THEMIS satellite location, we show the log-average hiss amplitude observed on THEMIS versus dipole $L$ and MLT in Figure 4a, along with the number of 4-s samples per 0.25-$R_E$/1-hr bin. Coverage of the plasmasphere is generally excellent, with an average of 2500 or more 4-s samples (spread across THEMIS probes A, D and E) per bin within $L = 7$ from June 2008–December 2010. Figure 4a shows that hiss is primarily a day-side phenomenon, appearing from dawn to dusk with a minimum in the midnight sector. At all local times, average hiss amplitude peaks around $L = 4$. Although bins with fewer than 120 s (30 measurements) have been excluded, a few high-amplitude artifacts appear at high $L$-shells, near MLT = 2 and MLT = 11 due to the low number of samples in those regions coincidentally taking place during periods of high hiss amplitude. We show the average of the log amplitude instead of the average linear amplitude [e.g., *Meredith et al.*, 2001, 2004] or the average

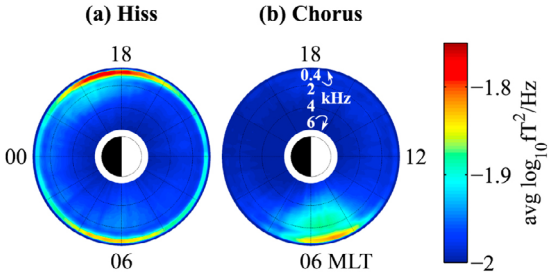


**Figure 3.** Cumulative spectrograms of chorus and hiss at Palmer Station, based on data from May 2000 through May 2010. Hiss is observed below 1 kHz at all local times, with bimodal peaks near dawn and dusk. Some additional higher-frequency structure up to ~3 kHz is observed in the dusk sector. Chorus is observed exclusively in the dawn sector up to ~6 kHz. This figure is analogous to Figure 7 of *Golden et al.* [2011], except that the latter used rectangular cumulative spectrograms instead of circular ones.

power (RMS amplitude) [e.g., *Li et al.*, 2009] because of the high dynamic range of hiss amplitude.

[31] When considering the ability to predict the observed hiss amplitude on a given THEMIS probe based on hiss observed at Palmer, we restrict ourselves to epochs where the dipole MLT of Palmer is within 1 hr of the dipole MLT of that THEMIS probe. We do not restrict measurements based on THEMIS $L$ due to the fact that magnetospheric waves may experience significant cross-$L$ propagation en route to the ground from their magnetospheric source [e.g., *Golden et al.*, 2010]. Of the total of 70,080 15-min synoptic epochs from 1 June 2008 through 31 May 2010, there were 1740 synoptic epochs in which Palmer recorded data and was within 1 hr MLT of one or more THEMIS probes which were within the plasmasphere and had SCM FBK data available which was above the instrument threshold. Although epochs where no hiss was detected on THEMIS above the instrument threshold were excluded, epochs where no hiss was detected at Palmer were *not* excluded, because this Boolean "hiss/no hiss at Palmer" value is a predictor in our model. Additionally, because we count measurements from each THEMIS probe independently and there were synoptic epochs during which Palmer was within 1 hr MLT of more than one THEMIS probe, a total of 1926 15-min measurements which meet the above criteria are available for use in this study.

**Table 1.** Distribution of Measurements

| | Palmer in Darkness | Palmer in Daylight |
|---|---|---|
| 00 < MLT < 12 | 218 | 643 |
| 12 < MLT < 24 | 23 | 1042 |

[32] As discussed previously in section 4.1, we separately consider statistics for when Palmer is in local daylight and local darkness, and for 00 < MLT < 12 and 12 < MLT < 24. Table 1 shows the number of measurements for the four models. Due to intricacies of the THEMIS ephemeris, only 23 measurements are available while Palmer is in darkness for 12 < MLT < 24; therefore, we discard this model, and we only model the other three scenarios which have a larger number of statistics. Far more samples exist while Palmer is in daylight than in darkness, partially because the ionosphere 100 km above Palmer is sunlit for the majority of the hours of a given year. Distributions of the THEMIS measurements during local darkness and local daylight at Palmer, as a function of $L$ and MLT, are shown in Figures 4b and 4c, respectively (samples while Palmer is in darkness for 12 < MLT < 24 are not shown). The best represented $L$ range is $2 < L < 3$, which is conveniently centered around Palmer's IGRF field line of $L = 2.4$. These sampling distributions were not our conscious choice; they may be considered a "coincidence," though they are deterministic based on the THEMIS ephemeris and Palmer's MLT.

### 4.3. THEMIS Hiss Amplitude as a Predictor of Hiss at Palmer

[33] Before we consider the ability for ground measurements of hiss to predict the in situ hiss environment, it is helpful to consider the inverse scenario, namely the extent to which measured in situ hiss amplitude may predict the presence of hiss on the ground. Our end goal is to predict in situ measurements from ground measurements, given our practical interest in using cheap ground measurements to estimate the space environment. Nonetheless, it is both

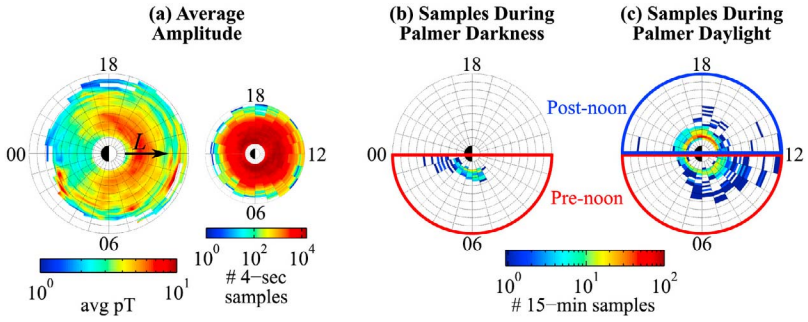


**Figure 4.** (a) Average amplitude of plasmaspheric hiss observed on THEMIS probes A, D and E from June 2008–December 2010 along with distribution of 4-s samples. Hiss amplitude values are linearly interpolated between bin centers (which is why they appear "smoothed"). Bins with fewer than 30 measurements have been excluded. (b) Distribution of samples used in this study when Palmer is in local darkness (only pre-noon samples are included). (c) Distribution of samples used in this study when Palmer is in local daylight. Bin sizes are 1 hr in MLT and 0.25 $R_E$ in $L$. Grid points with no data are white.

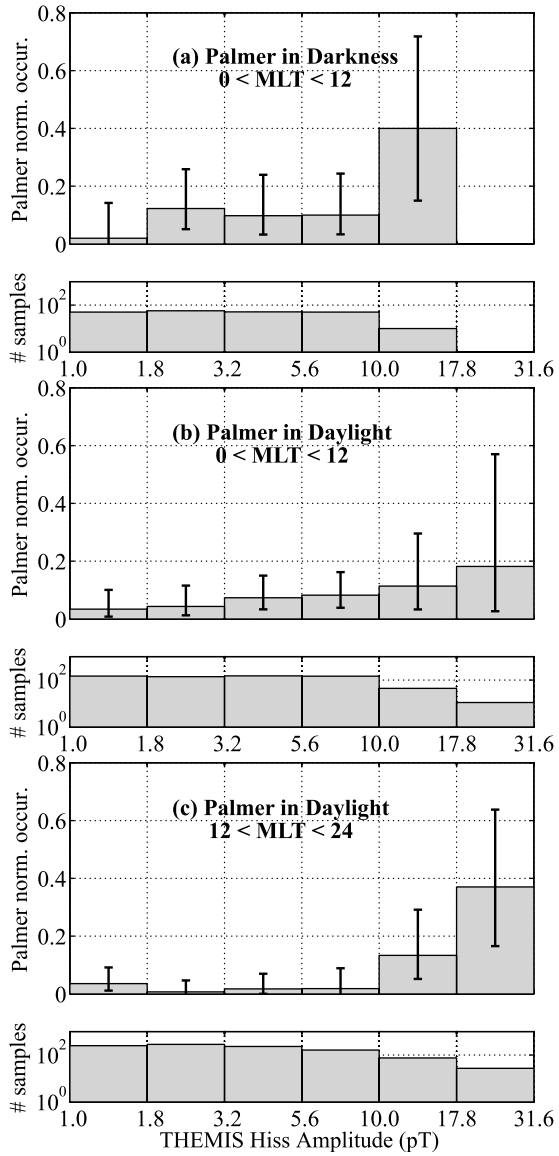


**Figure 5.** Normalized occurrence of observed hiss at Palmer as a function of THEMIS plasmaspheric hiss amplitude. Error bars are 95% confidence intervals.

intuitive and causal to do the reverse, namely to predict ground measurements from in situ measurements, as hiss emissions originate in space before propagating to the ground (even if terrestrial lightning is the source of hiss, the energy is not considered "hiss" until it is dispersed within the magnetosphere).

[34] The ability for measurements on THEMIS to predict the presence of hiss at Palmer is illustrated in Figure 5, which shows the normalized occurrence of hiss at Palmer, separately for our three models of Palmer solar illumination and MLT, as a function of in situ hiss amplitude observed on THEMIS. Below the normalized occurrence histograms, we also show the number of samples in each bin. Error bars shown are 95% confidence intervals using the Agresti-Coull binomial proportion confidence interval [*Agresti and Coull*, 1998] based on the "effective" number of samples for estimates of the mean of an autocorrelated time series [*Bayley and Hammersley*, 1946; *Mudelsee*, 2010, equation 2.7].

[35] It can be clearly seen from Figure 5 that hiss is observed significantly more often at Palmer when the in situ plasmaspheric hiss amplitude is greater. One may infer that, if these plots were extrapolated, hiss with very high in situ amplitude greater than 30 pT would show a high probability of being observed at Palmer under any scenario; however we do not have sufficient high-amplitude hiss data to verify this. The most profound difference between observations during local darkness and those during local daylight at Palmer is that lower-amplitude in situ emissions are more likely to be seen at Palmer during local darkness, as a result of the decreased ionospheric absorption when the ionosphere above Palmer is in darkness. Note that very few samples of high THEMIS hiss amplitudes are available, so it is difficult to compare the different solar illumination/MLT models for high THEMIS hiss amplitudes above 10 pT.

[36] Additional insight may be gained by examining the empirical cumulative distribution function (CDF) of THEMIS hiss amplitude. The empirical *complementary* CDF (defined as one minus the empirical CDF) of THEMIS hiss amplitude, as a function of whether hiss is or is not observed at Palmer, is shown in Figure 6. The complementary CDF is interpreted as the probability that the observed hiss amplitude is greater than or equal to the given hiss amplitude, given that hiss amplitude is above the THEMIS SCM noise floor. For example, Figure 6a indicates that, when Palmer is in darkness, there is a 14% chance of observing hiss with amplitude above 10 pT on THEMIS when hiss is observed at Palmer, versus a 3% chance when hiss is not observed at Palmer. On average, hiss is observed on THEMIS above the SCM noise floor in 84% of epochs, so these numbers may be considered absolute percentages if they are multiplied by 0.84. This sort of view of the data is convenient for making predictions about the minimum hiss amplitude given the presence of hiss or not at a ground station like Palmer. However, it should be cautioned that confidence bounds are difficult to calculate for autocorrelated data, given that standard formulas for empirical CDF confidence intervals assume independent measurements. Thus, the empirical complementary CDF shown in Figure 6 gives the likely mean of the true complementary CDF, but the uncertainty is unknown.

[37] Finally, we show the distribution of hiss amplitude on THEMIS when hiss is and is not seen at Palmer in Figure 7. Consistent with Figures 5 and 6, when Palmer is in daylight for 12 < MLT < 24 (Figure 7c), plasmaspheric hiss of high amplitudes is observed on THEMIS significantly more often when hiss is observed at Palmer than when hiss is not observed at Palmer. The dependence of the THEMIS hiss amplitude distributions on Palmer hiss occurrence for the two scenarios in the 00 < MLT < 24 sector (Figures 7a and 7b) are more subtle. These THEMIS amplitude distributions suggest that the ability for hiss at Palmer to predict high plasmaspheric hiss amplitudes may only be effective in the 12 < MLT < 24 sector. On average, hiss is only observed at Palmer for 4% of epochs in this study, which results in large error bars for the case when hiss *is* observed at Palmer due to the low number of samples.

[38] Note that we have not controlled for THEMIS ephemeris in Figures 5, 6, or 7. If, for example, the THEMIS

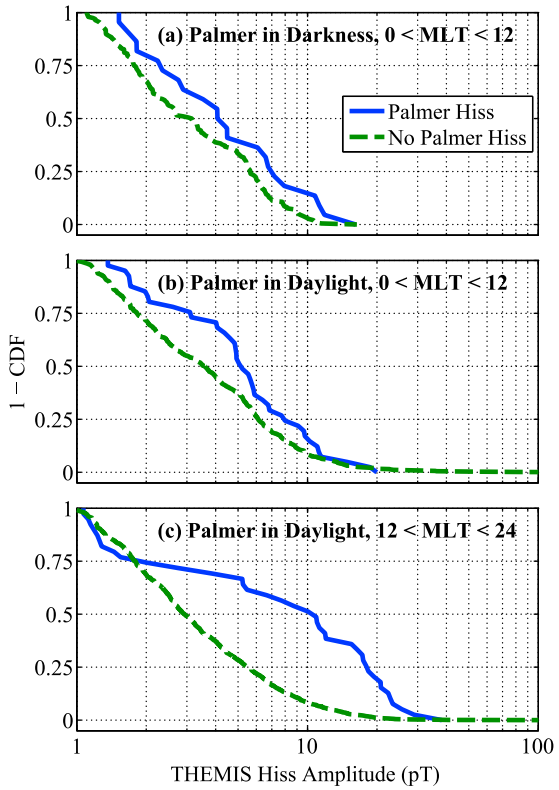


**Figure 6.** Empirical cumulative distribution functions of THEMIS plasmaspheric hiss amplitude when hiss either is (blue line) or is not (green line) observed at Palmer. These CDFs are conditioned on the fact that the observed hiss amplitude on THEMIS is above the instrument noise floor (which is true in 84% of measurements).

satellites were coincidentally in the region of peak hiss occurrence more often when hiss was observed at Palmer than when hiss was not observed at Palmer, these figures might erroneously suggest that hiss at Palmer was more predictive than it truly would be if the ephemeris distributions were equivalent. We control for THEMIS ephemeris in the ARMAX model for prediction of THEMIS hiss amplitude from Palmer data, discussed in section 4.4.2.

### 4.4. The ARMAX Model for Prediction of In Situ Hiss Amplitude

#### 4.4.1. Definition of the ARMAX Regression Model

[39] Our goal in this study is to statistically predict the amplitude of plasmaspheric hiss observed on THEMIS using only THEMIS ephemeris information and measurements of hiss on the ground. A standard statistical method of predicting a known quantity from a linear combination of potentially predictive measurements is via multiple regression. Under multiple regression, the quantity of interest (the "response"), $Y$, is modeled from a set of $P$ predictors, $X_1, X_2, \ldots, X_P$, as

$$Y = C + \beta_1 X_1 + \beta_2 X_2 + \cdots + \beta_P X_P + \varepsilon, \qquad (2)$$

where $C$ is a constant and $\varepsilon$ is a random error. The errors are assumed to be independent and identically distributed (i.i.d.) for the least squares solution to be optimal and unbiased and for accurate estimation of the uncertainty of the fit.

[40] A problem arises when attempting to model geophysical time series data, such as hiss amplitude, because of the time dependence of the measurements. It is assumed in (2) that measurements, and particularly errors, are i.i.d. However, successive satellite measurements of hiss amplitude are guaranteed to be autocorrelated; that is, a given measurement of hiss amplitude will always be very similar in magnitude to the previous measurement due to the fact that the measurement rate is fast when compared to the rate of satellite movement through the hiss region and the timescale of variation of hiss amplitude. This violates the assumption of independent measurements. It follows then that the model errors would be similarly autocorrelated. This is a serious problem; when the regression model has correlated errors, regression coefficients do not have minimum variance, estimates of the variance of the model error and uncertainty of model parameters may be significantly understated, and tests of significance of model parameters are not strictly valid [e.g., *Chatterjee and Hadi* 2006, section 8]. As a result, the model form of (2) is not appropriate for modeling time series data.

[41] However, a simple modification to (2) may be made to allow for an equivalent analysis for time series data. In

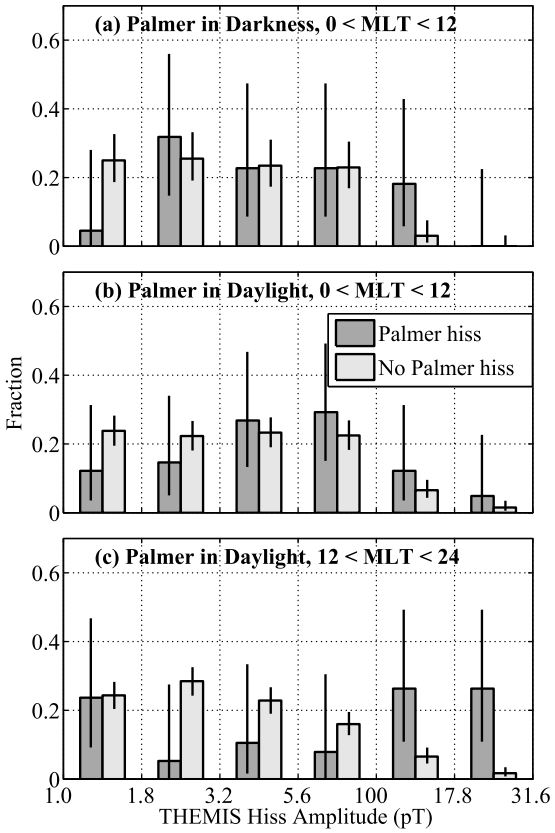


**Figure 7.** Distribution of plasmaspheric hiss amplitude observed on THEMIS when hiss is and is not observed at Palmer. Error bars are 95% confidence intervals. Note that, unlike in the ARMAX model results, this figure does not control for potentially different THEMIS ephemeris distributions when hiss is and is not seen at Palmer.

general, time series, such as measurements of plasmaspheric hiss, may be modeled as first order autoregressive, or AR(1) processes. Under this model, a measurement $Y_n$ at time $n$ is modeled as

$$Y_n = C + \alpha Y_{n-1} + \varepsilon_n \tag{3}$$

where $0 < \alpha < 1$ is the AR(1) coefficient and $\varepsilon_n$ is the i.i.d. error which depends on the inter-measurement change in the recorded data (this is distinct from the $\varepsilon$ error term in (2)). $\alpha$ is a measure of the interdependence of successive samples, where $\alpha = 1$ indicates perfect inter-sample correlation and $\alpha = 0$ indicates no inter-sample correlation. In general, for the same type of measurement, time series data which is sampled more finely will have a value of $\alpha$ nearer to 1. For example, 1-hr *AE* data from January 2000 through December 2010, collected from the World Data Center for Geomagnetism, Kyoto, has $\alpha = 0.84$, while 1-min *AE* data from the same time period has $\alpha = 0.9954$.

[42] The autoregressive aspect of the signal can be incorporated into the regression model to create an "autoregressive moving average with exogenous inputs" (ARMAX) model. In the ARMAX model, using a first-order autoregressive component, the response is modeled as

$$Y_n = C + \alpha Y_{n-1} + \varepsilon_n + \sum_{i=1}^{M} \theta_i \varepsilon_{n-i} + \sum_{k=1}^{P} \beta_k X_{n,k} \tag{4}$$

where $\varepsilon_{n-i}$ is the error at time $n-i$, $X_{n,k}$ is the $k$th exogenous predictor at time $n$, and the coefficients $C$, $\alpha$, $\theta_i$ and $\beta_k$ must all be estimated.

[43] The moving average (MA) component, $\sum_{i=1}^{M} \theta_i \varepsilon_{n-i}$, is not necessary for autoregressive time series, such as THEMIS measurements of plasmaspheric hiss, which can be described adequately using an AR(1) model; that is, the current measurement can be predicted based on the previous measurement, and additional measurement history does not significantly improve the prediction. This is the case with our hiss data, where each sample may be described as a "random" (though, to some extent, predictable) perturbation from the previous sample (an AR process), as opposed to a process where each sample is the weighted sum of a time history of random perturbations (an MA process). In practice, a finite order AR process may be described by an infinite order MA process and vice versa [*Chatfield*, 1996, section 3.4]. The MA component may be dropped from our model, yielding the reduced model,

$$Y_n = C + \alpha Y_{n-1} + \sum_{k=1}^{P} \beta_k X_{n,k} + \varepsilon_n. \tag{5}$$

We continue to refer to this model form as ARMAX, with the MA coefficients set to zero. The model form of (5) is that which is used in the statistical analysis described in section 4.4.2.

[44] We denote the ARMAX estimates of the response and coefficients with a hat; e.g., the estimated value of $Y_n$ is $\hat{Y}_n$. In the model of (5), the value of $Y_n$ depends on $Y_{n-1}$, the previous measurement of $Y$. In general, if we are attempting to predict hiss amplitude at a given point in space and time under known geomagnetic conditions, $Y_{n-1}$ will not be known. In this case, the best estimate of $Y_n$ will be given by

$$\hat{Y}_n = \hat{C} + \hat{\alpha} E(Y) + \sum_{k=1}^{P} \hat{\beta}_k X_{n,k} \tag{6}$$

where $\hat{C}$ and $\hat{\beta}_k$ are coefficient estimates determined previously from the known data and $E(Y)$ is the expected value (mean) of $Y$ over all $n$. $\hat{Y}_n$ is the unbiased best estimate of $Y_n$ when $Y_{n-1}$ is unknown. It is nonetheless important to estimate $\hat{C}$ and $\hat{\beta}_k$ using the ARMAX model of (5) instead of the simple multiple regression model of (2) because it is only when using the ARMAX model that the measures of uncertainty are valid.

#### 4.4.2. ARMAX Model Implementation and Results

[45] In our pursuit of a method to predict in situ hiss amplitude from ground measurements, we ask the question, "how much larger, on average, is in situ hiss amplitude when hiss is observed at Palmer, compared to when hiss is not observed at Palmer?" We can answer this question using the ARMAX model of (5). In this model, the response, $Y$, is the logarithm of the in situ hiss amplitude observed on THEMIS, and one of the predictors, $X_k$, is a Boolean indicator variable with a value of 1 when hiss is observed at Palmer and 0 when it is not. The logarithm of in situ hiss amplitude is used instead of the linear hiss amplitude to ensure that the distribution of the response is approximately Gaussian.

[46] Average hiss amplitude is also a function of THEMIS ephemeris, as shown in Figure 4, so predictors which are functions of $L$, MLT and $\lambda$ (magnetic latitude) must also be included as predictors in the model. Multiple regression is inherently a linear model, where the response is expected to be a linear function of the predictors. Therefore, to include ephemeris parameters as predictors in the model, we transform them into parameters on which we expect hiss amplitude to be linearly dependent (though perhaps weakly so). $L$, in units of $R_E$, is represented in the model as $|\ln(L-1) - \ln(3)|$, which takes into account the fact that average hiss amplitude peaks at $L = 4$ and that hiss amplitude should approach 0 as $L$ approaches either 1 (the surface of the Earth) or infinity. MLT, in units of hours, is represented as $\cos(\text{MLT}/24 * 2\pi)$ and $|\sin(\text{MLT}/24 * 2\pi)|$, which takes into account the fact that hiss amplitude peaks at noon and is approximately symmetric about the dawn/dusk line. Finally, $\lambda$, in units of radians, is included as $\cos(\lambda)$, under the expectation that hiss amplitude peaks either at the equator or at high latitudes (note that THEMIS measurements near the dipole equator have been excluded, as discussed in section 2.1).

[47] We use the ARMAX modeling procedure from the Matlab software package (MathWorks, Inc., Natick, MA) to implement the ARMAX model with an AR(1) component and no moving average term. The response is THEMIS hiss amplitude, in units of $\log_{10}$pT. The resulting coefficients ($\beta$), standard errors (SE), and $p$-values ($p$) for our three models are shown in Tables 2, 3, and 4. The $p$-value represents the probability of obtaining data equal to or more extreme than the recorded data if the given parameter's coefficient is actually 0. We take $p$-values less than or equal to 0.05 to represent "significant" variables, i.e., those that make a meaningful contribution to the model. Under this definition,

**Table 2.** ARMAX Predictors for Palmer in Darkness, 00 < MLT < 12

| Predictor | $\beta$ | SE | $p$ |
|---|---|---|---|
| Constant ($C$) | 3.420 | 3.032 | 0.261 |
| AR(1) | 0.133 | 0.068 | 0.050 |
| $\lvert\ln(L-1)-\ln(3)\rvert$ | 0.089 | 0.074 | 0.230 |
| abs(sin(MLT)) | −0.026 | 0.173 | 0.880 |
| cos(MLT) | 0.041 | 0.073 | 0.580 |
| cos($\lambda$) | −3.091 | 3.074 | 0.316 |
| Palmer Hiss (Bool) | 0.147 | 0.061 | 0.017 |

**Table 4.** ARMAX Predictors for Palmer in Daylight, 12 < MLT < 24

| Predictor | $\beta$ | SE | $p$ |
|---|---|---|---|
| Constant ($C$) | −2.344 | 1.585 | 0.140 |
| AR(1) | 0.350 | 0.028 | <0.001 |
| $\lvert\ln(L-1)-\ln(3)\rvert$ | −0.083 | 0.036 | 0.020 |
| abs(sin(MLT)) | 0.149 | 0.031 | <0.001 |
| cos(MLT) | −0.035 | 0.017 | 0.041 |
| cos($\lambda$) | 2.668 | 1.603 | 0.096 |
| Palmer Hiss (Bool) | 0.297 | 0.040 | <0.001 |

we see that various ephemeris parameters are not significant (i.e., have $p > 0.05$); however the ephemeris predictors are meant simply to ensure that ephemeris effects are not confounded with the Boolean Palmer hiss predictor, and their actual coefficients and $p$-values are not of primary interest. Although the constant term has a $p$-value which is greater than 0.05 in all three models, the constant term is always retained in the model.

[48] We are mainly interested in the Palmer hiss predictor. When Palmer is in darkness (Table 2), the Palmer hiss coefficient, which has a value of 0.147, indicates that, on average, when Palmer is in darkness, the observed hiss amplitude on THEMIS is $10^{0.147}$ or 1.4 times higher when hiss is observed at Palmer than when hiss is not observed at Palmer. Analogously, when Palmer is in daylight for 00 < MLT < 12 (Table 3), the observed hiss amplitude on THEMIS is 1.2 times higher when hiss is observed at Palmer, and when Palmer is in daylight for 12 < MLT < 24 (Table 3), the observed hiss amplitude on THEMIS is 2 times higher when hiss is observed at Palmer. The Palmer Boolean $p$-value is 0.173 when Palmer is in daylight for 00 < MLT < 12 (Table 3), indicating that Palmer as a predictor of THEMIS hiss amplitude is not statistically significant in this case; this contrasts with the highly significant $p$-value of < 0.001 when Palmer is in daylight for 12 < MLT < 24, suggesting a fundamental difference between the pre-noon and the post-noon hiss observed at Palmer. We discuss the implications of this result in the next section.

## 5. Discussion

[49] As shown in section 4.4.2, while Palmer is in daylight for 12 < MLT < 24 (Table 4), the presence of hiss at Palmer is a fairly good predictor of high plasmaspheric hiss amplitudes on THEMIS. In this model, observed hiss at Palmer indicates a doubling of the average in situ hiss amplitude compared with when hiss is not observed at Palmer. It is therefore surprising to find the performance of the model for when Palmer is in daylight for 00 < MLT < 12 (Table 3) to be so poor, despite the fact that the THEMIS $L$ distribution shown in Figure 4c is very similar for the two MLT periods (the distribution of $\lambda$, not shown, is also approximately the same for the two periods). In the model for when Palmer is in daylight and 00 < MLT < 12, the Palmer predictor is not even statistically significant ($p > 0.05$).

**Table 3.** ARMAX Predictors for Palmer in Daylight, 00 < MLT < 12

| Predictor | $\beta$ | SE | $p$ |
|---|---|---|---|
| Constant ($C$) | −0.350 | 2.125 | 0.869 |
| AR(1) | 0.200 | 0.032 | <0.001 |
| $\lvert\ln(L-1)-\ln(3)\rvert$ | −0.166 | 0.053 | 0.002 |
| abs(sin(MLT)) | 0.104 | 0.046 | 0.024 |
| cos(MLT) | 0.004 | 0.020 | 0.835 |
| cos($\lambda$) | 0.867 | 2.171 | 0.690 |
| Palmer Hiss (Bool) | 0.085 | 0.063 | 0.173 |

[50] This result suggests that the two hiss populations observed at Palmer centered at dawn and dusk are fundamentally different, with the dawn population probably not originating within the plasmasphere and therefore not present in our plasmaspheric THEMIS data. The hiss observed at dawn at Palmer may have originated as either "ELF hiss," a hiss emission which is observed primarily outside the plasmasphere [*Gurnett and O'Brien*, 1964; *Russell et al.*, 1972], or chorus emissions which have originated at high $L$-shells, where the equatorial gyrofrequency (and therefore, the frequency of generated chorus) is low [*Tsurutani and Smith*, 1974, 1977; *Burtis and Helliwell*, 1976]. If the emissions originated as chorus, they must have become sufficiently dispersed during the course of their propagation to low $L$-shells so as to arrive with minimal observable structure on the ground, which would cause them to be classified as "hiss" by our automated algorithm. It is possible that plasmaspheric hiss is not able to reach the ground at Palmer in the dawn sector due to variations in its magnetospheric wavenormal distribution with MLT; if this is the case, we expect that an situ survey would show more oblique plasmaspheric hiss wavenormals in the dawn sector and more field-aligned wavenormals in the dusk sector.

[51] In the best performing model (Palmer in daylight and 12 < MLT < 24, Table 4), the fact that the presence of hiss at Palmer predicts a doubling of the in situ hiss amplitude is compelling, but it is still somewhat modest given the 1.5 orders of magnitude range of observed hiss amplitudes on the THEMIS SCM instruments, from ∼1 pT (the instrument noise floor) to ∼35 pT (the 99th percentile of observed hiss amplitudes when the amplitude is above the instrument noise floor). However, we note that the predictive ability of our model may be hampered by the fact that the entire study period occurred during solar minimum, when the average $AE$ was only 87 nT. In contrast, in 2003, for example, during the declining phase of solar cycle 23, the average $AE$ was 328 nT, with emissions observed at Palmer more than six times as often as in 2009 [*Golden et al.*, 2011, Figure 9].

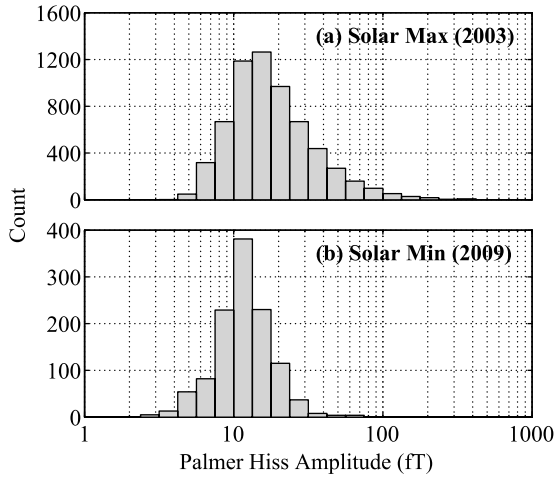


**Figure 8.** Distribution of hiss amplitude at Palmer during (a) 2003, a year during solar maximum with many geomagnetic disturbances, and (b) 2009, a year during solar minimum with very few geomagnetic disturbances, such as during this study. The median hiss amplitude during the two periods are similar, but the distribution during solar max has a much longer tail for high amplitude emissions.

[52] In Figure 8, we show the distribution of the amplitude of hiss emissions observed at Palmer during a year with many geomagnetic disturbances, 2003, contrasted with that from a quiet geomagnetic year, 2009, which is in the range of dates included in this study. The median amplitude is similar during both years, at 16 fT during 2003 versus 11 fT during 2009. However, the amplitude distribution during 2003 has a much longer tail for high amplitudes; the 95th percentile of amplitude is 22 fT in 2009 versus 63 fT in 2003. As shown previously in Figure 5, the probability of observing hiss at Palmer increases dramatically once in situ hiss amplitude rises above a certain threshold, and with more data points above that threshold, the likelihood that hiss emissions at Palmer are indicative of large amplitude in situ emissions will increase. We therefore believe that, if this study is repeated using additional data obtained during solar maximum, ground observations may prove to be a more effective predictor of in situ hiss amplitudes.

## 6. Summary

[53] Due to the high cost and low data rate of satellites used to observe plasmaspheric hiss in situ, ground stations are an appealing source of hiss observations which may be complimentary to those from satellites. However, observations of plasmaspheric hiss on the ground are limited to the subset of emissions which are able to propagate from their source in the magnetosphere with sufficiently mild attenuation to the ground; thus, ground data requires an additional layer of interpretation before it can be used to understand the space environment.

[54] In this study, we investigated how the average in situ hiss amplitude, as measured by the THEMIS spacecraft, changed when hiss either was or was not observed at Palmer Station, Antarctica. We found that, when hiss is observed at Palmer when the station is in daylight in the range $12 < \text{MLT} < 24$, the average hiss amplitude on THEMIS is 2 times higher than when hiss is not observed at Palmer. However, the presence of hiss at Palmer carries only a moderate 1.4 times increase in THEMIS hiss amplitude for the same MLT range when Palmer is in darkness, and it is not statistically significant when Palmer is in daylight in the range $00 < \text{MLT} < 12$. We explain that the discrepancy in predictive ability during the two MLT ranges may be due to the fact that, while hiss observed at Palmer for $12 < \text{MLT} < 24$ is plasmaspheric hiss, hiss observed at other MLTs may be a fundamentally different emission which originates outside the plasmasphere, such as ELF hiss or magnetospheric chorus. We believe that a model specified with data collected during years with both high and low geomagnetic activity may be more effective at predicting in situ hiss amplitude in the range $12 < \text{MLT} < 24$.

[55] **Acknowledgments.** This work was supported by the National Science Foundation under awards 1043442 and 1137411. *AE* data were obtained from the World Data Center for Geomagnetism, Kyoto. THEMIS data were obtained from NASA CDAWeb THEMIS database and we acknowledge NASA contract NAS5-02099 and V. Angelopoulos for use of data from the THEMIS Mission, as well as J. W. Bonnell and F. S. Mozer for use of EFI data, C. W. Carlson and J. P. McFadden for use of ESA data, A. Roux and O. LeContel for use of SCM data and C. Cully for use of FBK data.

[56] Robert Lysak thanks the reviewers for their assistance in evaluating this paper.

## References

Abel, B., and R. M. Thorne (1998), Electron scattering loss in Earth's inner magnetosphere: 1. Dominant physical processes, *J. Geophys. Res.*, *103*, 2385–2396, doi:10.1029/97JA02919.

Agresti, A., and B. A. Coull (1998), Approximate is better than "exact" for interval estimation of binomial proportions, *Am. Stat.*, *52*(2), 119–126.

Angelopoulos, V. (2008), The THEMIS Mission, *Space Sci. Rev.*, *141*, 5–34, doi:10.1007/s11214-008-9336-1.

Bayley, G. V., and J. M. Hammersley (1946), The "effective" number of independent observations in an autocorrelated time series, *J. R. Stat. Soc.*, *8*(2), 184–197.

Bonnell, J. W., F. S. Mozer, G. T. Delory, A. J. Hull, R. E. Ergun, C. M. Cully, V. Angelopoulos, and P. R. Harvey (2008), The Electric Field Instrument (EFI) for THEMIS, *Space Sci. Rev.*, *141*, 303–341, doi:10.1007/s11214-008-9469-2.

Bortnik, J., R. M. Thorne, and N. P. Meredith (2008), The unexpected origin of plasmaspheric hiss from discrete chorus emissions, *Nature*, *452*, 62–66, doi:10.1038/nature06741.

Bortnik, J., W. Li, R. M. Thorne, V. Angelopoulos, C. Cully, J. Bonnell, O. Le Contel, and A. Roux (2009), An observation linking the origin of plasmaspheric hiss to discrete chorus emissions, *Science*, *324*, 775–778, doi:10.1126/science.1171273.

Burtis, W. J., and R. A. Helliwell (1976), Magnetospheric chorus: Occurrence patterns and normalized frequency, *Planet. Space Sci.*, *24*, 1007–1010, doi:10.1016/0032-0633(76)90119-7.

Chatfield, C. (1996), *The Analysis of Time Series: An Introduction*, 5th ed., Chapman and Hall, Boca Raton, Fla.

Chatterjee, S., and A. S. Hadi (2006), *Regression Analysis by Example*, 4th ed., Wiley-Interscience, Hoboken, N. J.

Church, S. R., and R. M. Thorne (1983), On the origin of plasmaspheric hiss: Ray path integrated amplification, *J. Geophys. Res.*, *88*, 7941–7957.

Cohen, M. B., R. K. Said, and U. S. Inan (2010), Mitigation of 50–60 Hz power line interference in geophysical data, *Radio Sci.*, *45*, RS6002, doi:10.1029/2010RS004420.

Cully, C. M., R. E. Ergun, K. Stevens, A. Nammari, and J. Westfall (2008), The THEMIS digital fields board, *Space Sci. Rev.*, *141*, 343–355, doi:10.1007/s11214-008-9417-1.

Draganov, A. B., U. S. Inan, V. S. Sonwalkar, and T. F. Bell (1992), Magnetospherically reflected whistlers as a source of plasmaspheric hiss, *Geophys. Res. Lett.*, *19*, 233–236, doi:10.1029/91GL03167.

Dunckel, N., and R. A. Helliwell (1969), Whistler-mode emissions on the OGO 1 satellite, *J. Geophys. Res.*, *74*, 6371–6385, doi:10.1029/JA074i026p06371.

Golden, D. I., M. Spasojevic, and U. S. Inan (2009), Diurnal dependence of ELF/VLF hiss and its relation to chorus at L = 2.4, *J. Geophys. Res.*, *114*, A05212, doi:10.1029/2008JA013946.

Golden, D. I., M. Spasojevic, F. R. Foust, N. G. Lehtinen, N. P. Meredith, and U. S. Inan (2010), Role of the plasmapause in dictating the ground accessibility of ELF/VLF chorus, *J. Geophys. Res.*, *115*, A11211, doi:10.1029/2010JA015955.

Golden, D. I., M. Spasojevic, and U. S. Inan (2011), Determination of solar cycle variations of midlatitude ELF/VLF chorus and hiss via automated signal detection, *J. Geophys. Res.*, *116*, A03225, doi:10.1029/2010JA016193.

Green, J. L., S. Boardsen, L. Garcia, W. W. L. Taylor, S. F. Fung, and B. W. Reinisch (2005), On the origin of whistler mode radiation in the plasmasphere, *J. Geophys. Res.*, *110*, A03201, doi:10.1029/2004JA010495.

Gurnett, D. A. (1976), Plasma wave interactions with energetic ions near the magnetic equator, *J. Geophys. Res.*, *81*, 2765–2770, doi:10.1029/JA081i016p02765.

Gurnett, D. A., and T. B. Burns (1968), The low-frequency cutoff of ELF emissions, *J. Geophys. Res.*, *73*, 7437–7445, doi:10.1029/JA073i023p07437.

Gurnett, D. A., and B. J. O'Brien (1964), High-latitude geophysical studies with satellite Injun 3, 5, very low frequency electromagnetic radiation, *J. Geophys. Res.*, *69*, 65–89, doi:10.1029/JZ069i001p00065.

Helliwell, R. A. (1965), *Whistlers and Related Ionospheric Phenomena*, Stanford Univ. Press, Stanford, Calif.

Inan, U. S., and M. Gołkowski (2010), *Principles of Plasma Physics for Engineers and Scientists*, Cambridge Univ. Press, Cambridge, U. K.

Kennel, C. F., and H. E. Petscheck (1966), Limit on stably trapped particle fluxes, *J. Geophys. Res.*, *71*, 1–28.

Kennel, C. F., and R. M. Thorne (1967), Unstable growth of unducted whistlers propagating at an angle to the geomagnetic field, *J. Geophys. Res.*, *72*, 871–878.

Le Contel, O., et al. (2008), First results of the THEMIS search coil magnetometers, *Space Sci. Rev.*, *141*, 509–534, doi:10.1007/s11214-008-9371-y.

Li, W., R. M. Thorne, V. Angelopoulos, J. Bortnik, C. M. Cully, B. Ni, O. LeContel, A. Roux, U. Auster, and W. Magnes (2009), Global distribution of whistler-mode chorus waves observed on the THEMIS spacecraft, *Geophys. Res. Lett.*, *36*, L09104, doi:10.1029/2009GL037595.

Li, W., R. M. Thorne, J. Bortnik, Y. Nishimura, V. Angelopoulos, L. Chen, J. P. McFadden, and J. W. Bonnell (2010), Global distributions of suprathermal electrons observed on THEMIS and potential mechanisms for access into the plasmasphere, *J. Geophys. Res.*, *115*, A00J10, doi:10.1029/2010JA015687.

Lyons, L. R., and R. M. Thorne (1973), Equilibrium structure of radiation belt electrons, *J. Geophys. Res.*, *78*, 2142–2149, doi:10.1029/JA078i013p02142.

Lyons, L. R., R. M. Thorne, and C. F. Kennel (1972), Pitch-angle diffusion of radiation belt electrons within the plasmasphere, *J. Geophys. Res.*, *77*, 3455–3474.

Lysak, R. L., and Y. Song (2004), Propagation of Alfvén waves at the plasma sheet boundary layer, in *Substorms 7: Proceedings of the 7th International Conference on Substorms*, edited by T. Pulkinnen and N. Ganushkina, pp. 81–86, Finn. Meteorol. Inst., Helsinki.

McFadden, J. P., C. W. Carlson, D. Larson, M. Ludlam, R. Abiad, B. Elliott, P. Turin, M. Marckwordt, and V. Angelopoulos (2008), The THEMIS ESA plasma instrument and in-flight calibration, *Space Sci. Rev.*, *141*, 277–302, doi:10.1007/s11214-008-9440-2.

Meredith, N. P., R. B. Horne, and R. R. Anderson (2001), Substorm dependence of chorus amplitudes: Implications for the acceleration of electrons to relativistic energies, *J. Geophys. Res.*, *106*, 13,165–13,178, doi:10.1029/2000JA900156.

Meredith, N. P., R. B. Horne, R. M. Thorne, D. Summers, and R. R. Anderson (2004), Substorm dependence of plasmaspheric hiss, *J. Geophys. Res.*, *109*, A06209, doi:10.1029/2004JA010387.

Meredith, N. P., R. B. Horne, M. A. Clilverd, D. Horsfall, R. M. Thorne, and R. R. Anderson (2006a), Origins of plasmaspheric hiss, *J. Geophys. Res.*, *111*, A09217, doi:10.1029/2006JA011707.

Meredith, N. P., R. B. Horne, S. A. Glauert, R. M. Thorne, D. Summers, J. M. Albert, and R. R. Anderson (2006b), Energetic outer zone electron loss timescales during low geomagnetic activity, *J. Geophys. Res.*, *111*, A05212, doi:10.1029/2005JA011516.

Meredith, N. P., R. B. Horne, S. A. Glauert, and R. R. Anderson (2007), Slot region electron loss timescales due to plasmaspheric hiss and lightning-generated whistlers, *J. Geophys. Res.*, *112*, A08214, doi:10.1029/2007JA012413.

Meredith, N. P., R. B. Horne, S. A. Glauert, D. N. Baker, S. G. Kanekal, and J. M. Albert (2009), Relativistic electron loss timescales in the slot region, *J. Geophys. Res.*, *114*, A03222, doi:10.1029/2008JA013889.

Moldwin, M. B., M. F. Thomsen, S. J. Bame, D. J. McComas, and K. R. Moore (1994), An examination of the structure and dynamics of the outer plasmasphere using multiple geosynchronous satellites, *J. Geophys. Res.*, *99*, 11,475–11,482, doi:10.1029/93JA03526.

Mozer, F. S. (1973), Analysis of techniques for measuring DC and AC electric fields in the magnetosphere, *Space Sci. Rev.*, *14*, 272–313, doi:10.1007/BF02432099.

Mudelsee, M. (2010), *Climate Time Series Analysis: Classical Statistical and Bootstrap Methods*, 1st ed., Springer, New York.

Němec, F., O. Santolík, K. Gereová, E. Macúšová, Y. de Conchy, and N. Cornilleau-Wehrlin (2005), Initial results of a survey of equatorial noise emissions observed by the Cluster spacecraft, *Planet. Space Sci.*, *53*, 291–298, doi:10.1016/j.pss.2004.09.055.

Parrot, M., O. Santolík, D. Gurnett, J. Pickett, and N. Cornilleau-Wehrlin (2004), Characteristics of magnetospherically reflected chorus waves observed by CLUSTER, *Ann. Geophys.*, *22*, 2597–2606, doi:10.5194/angeo-22-2597-2004.

Pedersen, A., F. Mozer, and G. Gustafsson (1998), Electric field measurements in a tenuous plasma with spherical double probes, in *Measurement Techniques in Space Plasmas: Fields*, *Geophys. Monogr. Ser.*, vol. 103, edited by F. Pfaff, E. Borovsky, and T. Young, pp. 1–12, AGU, Washington, D. C., doi:10.1029/GM103p0001.

Roux, A., O. Le Contel, C. Coillot, A. Bouabdellah, B. de La Porte, D. Alison, S. Ruocco, and M. C. Vassal (2008), The search coil magnetometer for THEMIS, *Space Sci. Rev.*, *141*, 265–275, doi:10.1007/s11214-008-9455-8.

Russell, C. T., R. E. Holzer, and E. J. Smith (1969), OGO 3 observations of ELF noise in the magnetosphere: 1. Spatial extent and frequency of occurrence, *J. Geophys. Res.*, *74*, 755–777, doi:10.1029/JA074i003p00755.

Russell, C. T., R. E. Holzer, and E. J. Smith (1970), OGO 3 observations of ELF noise in the magnetosphere: 2. The nature of the equatorial noise, *J. Geophys. Res.*, *75*, 755–768, doi:10.1029/JA075i004p00755.

Russell, C. T., R. L. McPherron, and J. P. J. Coleman (1972), Fluctuating magnetic fields in the magnetosphere. I: ELF and VLF fluctuation, *Space Sci. Rev.*, *12*, 810–856, doi:10.1007/BF00173072.

Santolík, O., J. Chum, M. Parrot, D. A. Gurnett, J. S. Pickett, and N. Cornilleau-Wehrlin (2006), Propagation of whistler mode chorus to low altitudes: Spacecraft observations of structured ELF hiss, *J. Geophys. Res.*, *111*, A10208, doi:10.1029/2005JA011462.

Sheeley, B. W., M. B. Moldwin, H. K. Rassoul, and R. R. Anderson (2001), An empirical plasmasphere and trough density model: CRRES observations, *J. Geophys. Res.*, *106*, 25,631–25,642, doi:10.1029/2000JA000286.

Smith, A. J., and P. J. Jenkins (1998), A survey of natural electromagnetic noise in the frequency range f = 110 kHz at Halley station, Antarctica: 1. Radio atmospherics from lightning, *J. Atmos. Sol. Terr. Phys.*, *60*, 263–277, doi:10.1016/S1364-6826(97)00057-6.

Smith, A. J., R. B. Horne, and N. P. Meredith (2010), The statistics of natural ELF/VLF waves derived from a long continuous set of ground-based observations at high latitude, *J. Atmos. Sol. Terr. Phys.*, *72*, 463–475, doi:10.1016/j.jastp.2009.12.018.

Sonwalkar, V. S. (1995), Magnetospheric LF-, VLF-, and ELF-waves, in *Handbook of Atmospheric Electrodynamics*, pp. 407–460, CRC Press, Boca Raton, Fla.

Sonwalkar, V. S., and U. S. Inan (1989), Lightning as an embryonic source of VLF hiss, *J. Geophys. Res.*, *94*, 6986–6994, doi:10.1029/JA094iA06p06986.

Storey, L. R. O. (1953), An investigation of whistling atmospherics, *Philos. Trans. R. Soc. London A*, *246*, 113–141.

Thorne, R. M., and C. F. Kennel (1967), Quasi-trapped VLF propagation in the outer magnetosphere, *J. Geophys. Res.*, *72*, 857–870.

Thorne, R. M., E. J. Smith, R. K. Burton, and R. E. Holzer (1973), Plasmaspheric hiss, *J. Geophys. Res.*, *78*, 1581–1596, doi:10.1029/JA078i010p01581.

Thorne, R. M., S. R. Church, and D. J. Gorney (1979), On the origin of plasmaspheric hiss: The importance of wave propagation and the plasmapause, *J. Geophys. Res.*, *84*, 5241–5247.

Tsurutani, B. T., and E. J. Smith (1974), Postmidnight chorus: A substorm phenomenon, *J. Geophys. Res.*, *79*, 118–127, doi:10.1029/JA079i001p00118.

Tsurutani, B. T., and E. J. Smith (1977), Two types of magnetospheric ELF chorus and their substorm dependences, *J. Geophys. Res.*, *82*, 5112–5128.